Available online at www.sciencedirect.com
SCIENCE DIRECT®
International Journal of Heat and Mass Transfer 48 (2005) 3864–3879
International Journal of HEAT and MASS TRANSFER
www.elsevier.com/locate/ijhmt

Numerical prediction of turbulent convective heat transfer in mini/micro channels for carbon dioxide at supercritical pressure

Pietro Asinari *

Dipartimento di Energetica, Politecnico di Torino, Corso Duca degli Abruzzi 24, Zip Code 10129, Torino, Italy

Received 13 April 2004

Abstract

A new approach to take into account the effects of variable physical properties on turbulence is suggested. It allows to choose freely the turbulent closure model for conventional terms due to velocity fluctuations and to describe coherently the additional terms due to density fluctuations. Numerical calculations based on the suggested approach have been performed for carbon dioxide flowing within mini/micro channels under cooling conditions. The numerical predictions show that the effects due to density fluctuations are smaller than it could have been initially supposed and that the heat transfer impairment for mini/micro channels, which some experiments seem to highlight, is not completely explained by the considered model.

Keywords: Forced convection; Supercritical; Density fluctuations; Turbulence models; Cooling; Carbon dioxide

1. Introduction

Increasing attention to environmental issues induces to reconsider natural fluids, in particular carbon dioxide, as alternative refrigerants [1]. The high working pressure and the favorable heat transfer properties of carbon dioxide allow to use extruded flat tubes with circular/elliptical ducts, which have diameters much smaller than usual ducts ($d < 2$ mm) [2]. Size reduction justifies the conventional name of mini/micro channels. Inside each mini/micro channel, the gas cooling process takes place without phase change, since the working fluid is at a supercritical pressure.

The highest temperature at which condensation/evaporation occurs is known as the critical temperature. Both theoretical and experimental evidences exist which indicate that the idea of a definite critical point, with unambiguous critical temperature, pressure and volume is probably only an approximation; actually there appears to be a critical region [3]. For each supercritical pressure, the value of temperature at which the specific heat capacity reaches a peak is called pseudo-critical temperature T_{pc}. When the bulk temperature decreases below the pseudo-critical temperature for the considered supercritical pressure, the fluid instantaneously changes from a gas-like state to a liquid-like state [4]. This phenomenon effects both convective heat transfer [5] and turbulent diffusivities [6].

A comprehensive review of heat transfer and pressure drop characteristics in the critical region for carbon

* Tel.: +39 011 564 4413; fax: +39 011 564 4499.
E-mail address: pietro.asinari@polito.it

0017-9310/$ - see front matter © 2005 Elsevier Ltd. All rights reserved.
doi:10.1016/j.ijheatmasstransfer.2005.03.028

Nomenclature

A	surface (m^2)
b	dimensionless factor (–)
Bo	buoyancy parameter (–)
c_p	specific heat capacity ($J\,kg^{-1}\,K^{-1}$)
C	robust correlation coefficient (–)
d	diameter of mini/micro channel (m)
e	dimensionless error (–)
f	generic thermophysical properties
$\mathbf{F}$	corrective tensor due to density fluctuations (–)
g	acceleration due to gravity ($m\,s^{-2}$)
G	mass flow rate ($kg\,s^{-1}$)
Gr	Grashof number (–)
h	specific enthalpy ($J\,kg^{-1}$)
H	generic source term
$\mathbf{I}$	identity matrix (–)
k	turbulent kinetic energy ($J\,kg^{-1}$)
L	length of the mini/micro channel (m)
M	identifier of turbulent closure model
N	natural number
$\mathbb{N}^+$	set of positive natural numbers
p	pressure (Pa)
Pr	Prandtl number (–)
q	thermal flux ($W\,m^{-2}$)
$\mathbb{Q}$	set of fractional numbers
r	radial coordinate (m)
$\mathbb{R}$	set of real numbers
Re	Reynolds number (–)
$\mathbf{S}$	stress tensor ($N\,m^{-2}$)
T	temperature (K)
u	velocity component along axial direction ($m\,s^{-1}$)
v	velocity component along radial direction ($m\,s^{-1}$)
V	volume (m^3)
$\mathbf{w}$	velocity vector ($m\,s^{-1}$)
x	axial coordinate (m)
y	distance from the wall (m)
z	generic quantity

Greek symbols

α	convective heat transfer coefficient ($W\,m^{-2}\,K^{-1}$)
β	modified compressibility factor ($kg\,J^{-1}$)
δ	Kronecker symbol
ϵ	turbulent dissipation rate ($m^2\,s^{-3}$)
ϕ	correction factor due to density fluctuations (–)
φ	non-ideal gas parameter (–)
Φ	rounding function
λ	thermal conductivity ($W\,m^{-1}\,K^{-1}$)
μ	dynamic viscosity ($N\,s\,m^{-2}$)
η	radial location of pseudo-critical temperature (m)
ω	generic solving variable
Ω	computational domain
ρ	density ($kg\,m^{-3}$)
σ	intensity index ($J\,kg^{-1}$)
θ	temperature difference (K)
χ	ratio of geometric progression (–)
ζ	sign of enthalpy gradient (–)

Subscripts and superscripts

a	axial/center-line condition
b	bulk condition
BR	Bellmore and Reid
c	critical condition
exp	experimental condition
l	laminar condition
L	referring to whole length of mini/micro channel
λ	referring to thermal conductivity
m	minimum value
μ	referring to dynamic viscosity
RNG	RNG k–ϵ model
SKE	standard k–ϵ model
t	turbulent condition
T	total/stagnation condition
w	wall condition

Notation

∂_x	partial derivative along axial direction = $\partial/\partial x$
∂_r	partial derivative along radial direction = $\partial/\partial r$
$\mathbf{z_1} \otimes \mathbf{z_2}$	diadic product
$\langle z \rangle \equiv \bar{z}$	time averaging

dioxide can be found in [7]. Krasnoshchekov et al. [8] carried out the first experimental study on heat transfer characteristics during turbulent flow in a horizontal tube with carbon dioxide at supercritical pressure under cooling conditions. Baskov et al. [9] found that their measurements for vertical tube were systematically lower than those calculated using the previous formula. Petrov and Popov [10] numerically developed a correlation for configurations where free convection is negligible and found good agreement with experimental data. More recently, Pettersen et al. [11] experimentally found for extruded flat tubes with mini/micro channels and carbon dioxide at supercritical pressure that a usual correlation, originally developed for constant properties, can

be suitably applied. Pitla et al. [12] proposed that this conventional correlation can be improved by averaging the results obtained with constant properties evaluated at both wall and bulk temperatures. Finally, Yoon et al. [15] found that all previous studies generally under-predict their measurements and proposed a new phenomenological correlation, which adopts the same functional dependence originally proposed by Krasnoshchekov et al. [8].

Liao and Zhao [13] investigated a single horizontal mini/micro channel with supercritical carbon dioxide and found that size reduction causes a heat transfer impairment, which cannot be predicted by correlations developed for normal-sized ducts. Liao and Zhao [13] measured the variation of Nusselt number Nu_b with the bulk mean temperature for various tube diameters, keeping the Reynolds number Re_b, the Prandtl number Pr_b and the difference between the bulk and wall temperature fixed. The Nusselt number was found to decrease as the tube size became smaller and this means that a heat transfer impairment due to size reduction could exist. Liao and Zhao pointed out that buoyancy effects could be responsible for this phenomenon. Theoretical considerations lead to the following criterion for negligible buoyancy effects in horizontal tubes [14]:

$$\frac{Gr}{Re_b^2} = \left(\frac{\rho_w}{\rho_b} - 1\right)\frac{gd}{u_b^2} < 1 \times 10^{-3}. \quad (1)$$

The Grashof number Gr represents the relative strength of secondary flow induced by the buoyancy force. Considering that the buoyancy parameter Gr/Re_b^2 is proportional to the tube diameter d, for each operative configuration a critical diameter exists and all tubes characterized by smaller diameters are free of buoyancy effects. Liao and Zhao found that, for their experimental tests, this critical diameter is comparable to the diameter, which conventionally constitutes the upper limit for mini/micro channels. They conclude that the heat transfer impairment could be caused, partially at least, by the fact that the buoyancy effect becomes less important for small tubes. In particular, in the region near the pseudo-critical temperature, the experimental data show wall thermal fluxes much lower than those predicted by the correlation of Petrov and Popov [10]. Liao and Zhao suggest that the correlation fails when free convection becomes weak or absent, because it was developed based on data for large-diameter tubes where this effect should be significant.

This explanation is not completely satisfactory. For horizontal tubes, buoyancy causes circumferential variations of heat transfer [5]. Some evidences exist that buoyancy reduces the total heat transfer in horizontal tubes, though not in a very pronounced manner [6]. Firstly, if tested mini/micro channels are characterized by negligible buoyancy effects, a small increase of heat transfer should be expected comparing with large-diameter tubes, contrary to experimental data. Secondly the correlation of Petrov and Popov does not take into account buoyancy effects. In a preliminary work, Petrov and Popov [16] numerically solved a system of equations which included also buoyancy in order to reproduce the experimental results of Baskov et al. [9], but, in the original paper, where their correlation was proposed, the buoyancy was dropped from the system of equations and no buoyancy parameter was included in the final interpolation formula [10]. The effect of free convection was considered only in a following paper [17].

According to experimental data, mini/micro channels for the considered conditions reveal a peculiar behavior in comparison with large-diameter tubes, i.e. heat transfer impairment, which has not been completely explained yet. Following the work of Petrov and Popov, the present work aims to numerically investigate the turbulent convective heat transfer in mini/micro channels for carbon dioxide at supercritical pressure. A new approach to take into account the effects of variable physical properties on turbulence is proposed, in order to widen the available numerical tools. Three numerical models are solved for a set of operating conditions which is wide enough for testing their suitability to explain heat transfer impairment in considered conditions. Finally, a comparison with phenomenological correlations developed for normal-sized ducts is also reported.

2. Physical models

2.1. Conventional approaches

Since the explanation of Liao and Zhao for heat transfer impairment lies on the fact that buoyancy is negligible for some working conditions of mini/micro channels, in the following only pure forced convective regime will be considered. This means that the limiting condition given by Eq. (1) is exactly verified.

Because of size reduction, the ratio between surface roughness and characteristic diameter increases. Experimental data for aluminum mini/micro channels, with the smallest diameter considered in the following, show only negligible discrepancies (6%) between measured pressure drops and Blasius's correlation, which was developed for hydraulically smooth regime [11]. It is reasonable to suppose that stainless steel mini/micro channels considered by Liao and Zhao were characterized by lower roughness and they can be considered hydraulically smooth over the entire investigated range of Reynolds numbers.

Turbulent forced convection heat transfer is described by the instantaneous conservation equations of continuity, momentum and energy. When the physical properties rapidly change with temperature, as happens near the critical point, the turbulent regime is characterized by high-frequency fluctuations of physical proper-

ties, in addition to the usual fluctuations of velocity components and temperature. Reynolds averaging, i.e. time averaging, of governing equations produces additional unknown quantities, which must be calculated in terms of solving variables. In particular, effects due to density are stronger than those due to diffusivities, such as dynamic viscosity and thermal conductivity [18].

On introducing the Reynolds decomposition for velocity $\mathbf{u} = \bar{\mathbf{u}} + \mathbf{u}'$ and density $\rho = \bar{\rho} + \rho'$ into instantaneous conservation equations and time-averaging the results, the governing equations of continuity, momentum and energy are obtained, namely

$$\nabla \cdot [\bar{\rho}(\bar{\mathbf{u}} + \bar{\mathbf{u}}^*)] = 0, \tag{2}$$

$$\nabla \cdot [\bar{\rho}\bar{\mathbf{u}} \otimes (\bar{\mathbf{u}} + \bar{\mathbf{u}}^*)] = -\nabla p + \nabla \cdot \mathbf{S}, \tag{3}$$

$$\nabla \cdot \left[\bar{\rho}\overline{h_{\mathrm{T}}}(\bar{\mathbf{u}} + \bar{\mathbf{u}}^*)\right] = -\nabla \cdot \mathbf{q} + \nabla \cdot (\mathbf{S}\bar{\mathbf{u}}), \tag{4}$$

where $\bar{\mathbf{u}}^* = \overline{\rho'\mathbf{u}'}/\bar{\rho}$ is the characteristic velocity for density fluctuations, $\mathbf{S} = \mathbf{S}^{\mathrm{l}} + \mathbf{S}^{\mathrm{t}}$ is the effective stress tensor and $\mathbf{q} = \mathbf{q}^{\mathrm{l}} + \mathbf{q}^{\mathrm{t}}$ is the effective thermal flux. Laminar and turbulent components for both effective stress tensor and effective thermal flux are defined as follow

$$\mathbf{S}^{\mathrm{l}} = \mu(\nabla\bar{\mathbf{u}} + \nabla\bar{\mathbf{u}}^{\mathrm{T}}) - (2/3\mu\nabla \cdot \bar{\mathbf{u}})\mathbf{I}, \tag{5}$$

$$\mathbf{S}^{\mathrm{t}} = -\bar{\rho}\overline{\mathbf{u}' \otimes \mathbf{u}'} - \overline{\rho'\mathbf{u}'} \otimes \bar{\mathbf{u}} - \overline{\rho'\mathbf{u}' \otimes \mathbf{u}'}, \tag{6}$$

$$\mathbf{q}^{\mathrm{l}} = -\lambda\nabla T, \tag{7}$$

$$\mathbf{q}^{\mathrm{t}} = \bar{\rho}\overline{h'_{\mathrm{T}}\mathbf{u}'} + \overline{\rho' h'_{\mathrm{T}}}\bar{\mathbf{u}} + \overline{\rho' h'_{\mathrm{T}}\mathbf{u}'}. \tag{8}$$

The last equation can be easily simplified by neglecting the difference between stagnation enthalpy and simple enthalpy. Some of the previous terms due to turbulent fluctuations can be expressed by defining turbulent viscosity and gradient-diffusion (see [19] for details), namely

$$-\bar{\rho}\overline{\mathbf{u}' \otimes \mathbf{u}'} = (\mu_{\mathrm{t}}/\mu)\mathbf{S}^{\mathrm{l}}, \tag{9}$$

$$\bar{\rho}\overline{h'\mathbf{u}'} = (\lambda_{\mathrm{t}}/\lambda)\mathbf{q}^{\mathrm{l}}. \tag{10}$$

A tensor $\mathbf{F}^{\mu}$ can be introduced to describe the effects due to density fluctuations on the effective stress tensor $\mathbf{S} = (\mathbf{I} + \mu_{\mathrm{t}}/\mu\mathbf{F}^{\mu})\mathbf{S}^{\mathrm{l}}$. In the same way, a tensor $\mathbf{F}^{\lambda}$ can be introduced to describe the effects due to density fluctuations on the effective thermal flux $\mathbf{q} = (\mathbf{I} + \lambda_{\mathrm{t}}/\lambda\mathbf{F}^{\lambda})\mathbf{q}^{\mathrm{l}}$, namely

$$\mathbf{F}^{\mu} = \mathbf{I} + \left(\overline{\rho'\mathbf{u}'} \otimes \bar{\mathbf{u}} + \overline{\rho'\mathbf{u}' \otimes \mathbf{u}'}\right)\left(\bar{\rho}\overline{\mathbf{u}' \otimes \mathbf{u}'}\right)^{-1}, \tag{11}$$

$$\mathbf{F}^{\lambda} = \mathbf{I} + \left(\overline{\rho' h'}\bar{\mathbf{u}} + \overline{\rho' h'\mathbf{u}'}\right) \otimes \overline{h'\mathbf{u}'} \Big/ \left(\bar{\rho}\overline{h'\mathbf{u}'} \cdot \overline{h'\mathbf{u}'}\right). \tag{12}$$

In particular, density fluctuations effect both diffusive and convective terms into Eqs. (2)–(4). Since $\mathbf{F}^{\mu}$ is not symmetric, then the effective stress tensor $\mathbf{S}$ is not symmetric either.

Keeping in mind the geometrical configuration realized by mini/micro channels, a two-dimensional computational domain $\Omega \in \mathbb{R}^2$ will be considered and a set of cylindrical coordinates will be adopted to describe it, namely $\Omega = \{(x, r) \in \mathbb{R}^2 : 0 \leqslant x \leqslant L,\ 0 \leqslant r \leqslant R\}$. The velocity vector components will be accordingly renamed $\bar{\mathbf{u}} = (\bar{u}, \bar{v})$. Even though the problem concerned can have local distortions and variations in the velocity and temperature field, the boundary layer theory [20] can be considered as a preliminary modeling approach in order to reduce the computational demand and to increase the number of simulations needed by statistical regression. Because of these simplifying assumptions, the momentum and energy equation can be simplified to yield the following expressions

$$\nabla_{xr} \cdot [\bar{\rho}(\bar{\mathbf{u}} + \bar{\mathbf{u}}^*)] = 0, \tag{13}$$

$$\nabla_{xr} \cdot [\bar{\rho}\bar{u}(\bar{\mathbf{u}} + \bar{\mathbf{u}}^*)] = -\frac{\mathrm{d}p}{\mathrm{d}x} + \frac{1}{r}\frac{\partial}{\partial r}(rS_{xr}), \tag{14}$$

$$\nabla_{xr} \cdot \left[\bar{\rho}\overline{h_{\mathrm{T}}}(\bar{\mathbf{u}} + \bar{\mathbf{u}}^*)\right] = +\frac{1}{r}\frac{\partial}{\partial r}(r\bar{u}S_{rx} - rq_r). \tag{15}$$

Simplifying the laminar stress tensor, then all the components of effective stress tensor can be expressed in terms of the transverse velocity gradient. In the same way, all the components of effective thermal flux can be expressed in terms of transverse temperature gradient. The previous simplifications yield

$$\mathbf{S} \approx \begin{bmatrix} \mu^{\mathrm{t}}F^{\mu}_{xr}\partial_r\bar{u} & (\mu + \mu^{\mathrm{t}}F^{\mu}_{xx})\partial_r\bar{u} \\ (\mu + \mu^{\mathrm{t}}F^{\mu}_{rr})\partial_r\bar{u} & \mu^{\mathrm{t}}F^{\mu}_{rx}\partial_r\bar{u} \end{bmatrix}, \tag{16}$$

$$\mathbf{q} \approx \left[\lambda^{\mathrm{t}}F^{\lambda}_{xr}\partial_r T, (\lambda + \lambda^{\mathrm{t}}F^{\lambda}_{rr})\partial_r T\right]^{\mathrm{T}}. \tag{17}$$

In the following some components of the tensors, which describe density fluctuations, are reported because they are involved in the calculation of effective diffusive terms S_{xr}, S_{rx} and q_r in simplified Eqs. (14) and (15), namely

$$F^{\mu}_{xx} = 1 + \frac{\overline{\rho'u'}\bar{v}}{\bar{\rho}\overline{u'v'}} + \frac{\overline{\rho'u'v'}}{\bar{\rho}\overline{u'v'}}, \tag{18}$$

$$F^{\mu}_{rr} = 1 + \frac{\overline{\rho'v'}\bar{u}}{\bar{\rho}\overline{u'v'}} + \frac{\overline{\rho'u'v'}}{\bar{\rho}\overline{u'v'}}, \tag{19}$$

$$F^{\lambda}_{rr} = 1 + \frac{\overline{\rho'h'}\bar{v}}{\bar{\rho}\overline{h'v'}} + \frac{\overline{\rho'h'v'}}{\bar{\rho}\overline{h'v'}}. \tag{20}$$

The off-diagonal components of the effective stress tensor may differ, i.e. $S_{xr} \neq S_{rx}$, because in general $F^{\mu}_{xx} \neq F^{\mu}_{rr}$. The term F^{μ}_{xx} directly effects the turbulent viscosity, while the term F^{μ}_{rr} describes the effect of density fluctuations on viscous heating, which can be usually neglected. For this reason, all considered models assume $F^{\mu}_{rr} \approx 1$ and consequently $S_{rx} \approx (1 + \mu_{\mathrm{t}}/\mu)S^{\mathrm{l}}_{rx} = (1 + \mu_{\mathrm{t}}/\mu)S^{\mathrm{l}}_{xr}$.

In order to quantify the importance of the density fluctuations along radial direction, an auxiliary radial velocity $\bar{v}_0$ is introduced, which represents the radial velocity field obtained neglecting density fluctuations. Assuming fixed the mean density distribution, this auxiliary function satisfies the following equation

$$\frac{\partial}{\partial x}(\bar{\rho}\bar{u}) + \frac{1}{r}\frac{\partial}{\partial r}(r\bar{\rho}\bar{v}_0) = 0. \tag{21}$$

Along the axial direction, the effect of density fluctuations can be clearly neglected $|\bar{u}^*| \ll |\bar{u}|$. Along radial direction, considering Eqs. (13) and (21) and applying proper boundary conditions, a relation among actual, characteristic and auxiliary radial velocities can be found $\bar{v} + \bar{v}^* = \bar{v}_0$. In the region near the critical point, strong density fluctuations ensure $|\bar{v}^*| \gg |\bar{v}_0|$. For all the following calculations, this condition has been verified for at least one order of magnitude. In this case, an easier correlation yields $\bar{v} + \bar{v}^* \approx 0$ and it can be applied to simplify Eqs. (18) and (20).

Finally, density fluctuations must be related to velocity fluctuations involved into turbulence closure models. The key idea is to expand the equation of state $\rho(h,p)$ by considering fluctuations of independent variables $\rho' = \partial_h\bar{\rho}|_p h' + \partial_p\bar{\rho}|_h p'$. Neglecting pressure variations, the residual term can be expressed by means of a modified compressibility $\beta = -\partial_h\bar{\rho}|_p/\bar{\rho}$, in order to find the final correlation $\rho' = -\bar{\rho}\beta h'$. This correlation can be applied into the definition of characteristic velocity due to density fluctuations $\bar{\mathbf{u}}^* = -\beta\overline{h'\mathbf{u}'}$, which influences the convective terms, and into the definitions of correction factors F^{μ}_{xx} and F^{λ}_{rr}, which influence the diffusive terms, and are defined as

$$F^{\mu}_{xx} = 1 - \beta^2\frac{\overline{h'u'h'v'}}{\overline{u'v'}} - \beta\frac{\overline{h'u'v'}}{\overline{u'v'}}, \tag{22}$$

$$F^{\lambda}_{rr} = 1 - \beta^2\overline{h'h'} - \beta\frac{\overline{h'h'v'}}{\overline{h'v'}}. \tag{23}$$

How physical properties varying with temperature influence the turbulent diffusivity expressions has not been systematically investigated [6]. Therefore, many different assumptions have been proposed for models based on the mixing length concept, which were originally developed for fluids with constant properties [20]. Semi-empirical correlations exist which express turbulent diffusivities as functions of a dimensionless distance from the wall $y^+ = (R-r)\sqrt{\bar{\rho}_x\tau_w}/\mu_x$, which can be useful to characterize the fluid–wall interaction [20]. Some authors assumed that the original correlations may be used without changes, if proper values of physical properties are considered to compute dimensionless distance y^+ [21–23].

Petrov and Popov applied the mixing length model to calculate the turbulent diffusivities. They considered an additional corrective procedure to compute effective values, based on the discrepancies between shear stresses computed with constant and variable properties. They totally neglected the effects due to density fluctuations and so implicitly assumed $F^{\mu}_{xx} = F^{\lambda}_{rr} = 1$.

Bellmore and Reid applied the mixing length model too and adopted an integral formulation in order to take into account variable thermophysical properties [24]. They proposed an innovative method to include density fluctuations in the equations of turbulent transport based on mixing length theory. The mixing length theory is based on two heuristic assumptions [20]

$$\langle u'v'\rangle = +C_{uv}\langle|u'|\rangle\langle|v'|\rangle, \tag{24}$$

$$\langle h'v'\rangle = -\zeta C_{hv}\langle|h'|\rangle\langle|v'|\rangle, \tag{25}$$

where $\zeta = \partial_r\bar{h}/|\partial_r\bar{h}|$, $0 < C_{uv} < 1$ and $0 < C_{hv} < 1$. The signs in both expressions are due to experimental evidence. In particular the sign in Eq. (24) depends on the fact that v is the velocity component aligned along the radial direction pointing towards the wall. The coefficients C_{uv} and C_{hv} are called robust correlation coefficients. Each average absolute deviation can be expressed by transverse velocity gradient or transverse enthalpy gradient: this means $\langle|u'|\rangle = l_u|\partial_r\bar{u}|$, $\langle|v'|\rangle = l_v|\partial_r\bar{u}|$ and $\langle|h'|\rangle = l_h|\partial_r\bar{h}|$. Introducing these expressions into the previous assumptions given by Eqs. (24) and (25) and grouping the unknown terms, two essential quantities emerge: the mixing length $l_m = (C_{uv}l_u l_v)^{1/2}$ and the turbulent Prandtl number $Pr_t = C_{uv}l_u/(C_{hv}l_h)$, namely

$$\langle u'v'\rangle = l_m^2|\partial_r\bar{u}|^2, \tag{26}$$

$$\langle h'v'\rangle = -\zeta(l_m^2/Pr_t)|\partial_r\bar{h}||\partial_r\bar{u}|. \tag{27}$$

Both quantities are supplied by turbulence closure models, based on the mixing length concept. Bellmore and Reid essentially interpreted the definitions of correlation coefficients due to robust statistics in a factorized form and this yields

$$\langle u'v'\rangle = \Delta u\Delta v, \tag{28}$$

$$\langle h'v'\rangle = \Delta h\Delta v, \tag{29}$$

where $\Delta u = b_1\langle|u'|\rangle$, $\Delta v = b_2\langle|v'|\rangle$ and $\Delta h = -\zeta b_3\langle|h'|\rangle$. The congruence with the original heuristic assumptions implies that $b_1 b_2 = C_{uv}$ and $b_2 b_3 = C_{hv}$ but these constraints are not sufficient to unambiguously determine the constants b_i. Eq. (26) suggests that the velocity fluctuations along both directions produce comparable effects. The condition $\Delta u = \Delta v$ allows us to produce an additional constraint $b_1 l_u = b_2 l_v$. In this way, the values of the constants are found, namely $b_1 = (C_{uv}l_v/l_u)^{1/2}$, $b_2 = (C_{uv}l_u/l_v)^{1/2}$ and $b_3 = C_{hv}C_{uv}^{-1/2}(l_v/l_u)^{1/2}$. The main advantage of recasting Eqs. (28) and (29) is that each function Δo depends only on the fluctuations of the same variable o' and it can be calculated by means of the mixing length theory. In analogy with this factorization, Bellmore and Reid proposed the following general decomposition

$$\langle(u')^{n_1}(v')^{n_2}(h')^{n_3}\rangle = (\Delta u)^{n_1}(\Delta v)^{n_2}(\Delta h)^{n_3}, \tag{30}$$

where $n_i \in \mathbb{N}^+$. For example, considering $n_1 = n_3 = 1$ and $n_2 = 0$, the expression for turbulent thermal diffusivity along axial direction can be found, namely

$$\langle h'u'\rangle = \Delta h\Delta u = -\zeta(C_{hv}l_v/l_u)\langle|h'|\rangle\langle|u'|\rangle = -\zeta C_{hu}\langle|h'|\rangle\langle|u'|\rangle. \quad (31)$$

Similarly we can proceed with all turbulent terms involved into Eqs. (22) and (23), which can be calculated by means of the general decomposition given by Eq. (30). Recalling Eqs. (29) and (31), the characteristic velocity due to density fluctuations can be expressed as

$$F^{\mu}_{xx} = F^{\lambda}_{rr} = \phi_{\mathrm{BR}} = 1 + \zeta\beta\sigma_{\mathrm{BR}} - \beta^2\sigma^2_{\mathrm{BR}}, \quad (32)$$

$$\bar{u}^*_{\mathrm{BR}} = \bar{v}^*_{\mathrm{BR}} = \zeta\beta\left(l^2_{\mathrm{m}}|\partial_r\bar{u}|/Pr_{\mathrm{t}}\right)|\partial_r\bar{h}|, \quad (33)$$

where $\sigma_{\mathrm{BR}} = (l_{\mathrm{m}}/Pr_{\mathrm{t}})|\partial_r\bar{h}|$ can be considered an index of intensity for density fluctuations. We can now discuss the effects due to density fluctuations. Since $\beta\sigma_{\mathrm{BR}}$ is usually a small quantity also near the critical point, we can suppose $\phi_{\mathrm{BR}} \approx 1 + \zeta\beta\sigma_{\mathrm{BR}}$. This means that during cooling conditions ($\zeta < 0$), density fluctuations reduce turbulent diffusivities ($\phi_{\mathrm{BR}} < 1$), while during heating conditions ($\zeta > 0$) they substantially increase turbulent diffusivities ($\phi_{\mathrm{BR}} > 1$). Additional convective terms along the axial direction are negligible. The radial velocity field in absence of density fluctuations $\bar{v}_0$ can be discussed by Eq. (21). Let us define a vectorial velocity in the absence of density fluctuations $\bar{\mathbf{u}}_0 = (\bar{u}, \bar{v}_0)$. For mini/micro channels, the density gradient can be reasonably assumed orthogonal to this velocity $\bar{\mathbf{u}}_0 \cdot \nabla\rho \approx 0$, because $\bar{\mathbf{u}}_0$ is approximately oriented along streamlines. In this way, Eq. (21) easily yields that $-\zeta\bar{v}_0 \geqslant 0$. Recalling that $\bar{v} \approx -\bar{v}^*$ and $\zeta\bar{v}^* \propto (\partial_r\bar{h})^2 \geqslant 0$ by definition, a similar correlation for the effective radial velocity is found $-\zeta\bar{v} \geqslant 0$. Since $|\bar{v}| \gg |\bar{v}_0|$, then density fluctuations increase convective radial terms both during cooling conditions ($\bar{v} \gg \bar{v}_0 \geqslant 0$) and heating conditions ($\bar{v} \ll \bar{v}_0 \leqslant 0$).

2.2. Proposed turbulence closure model

Both previous models use turbulent models based on the mixing length concept and they have some drawbacks [19]. Firstly, they strongly depend on the geometry of the considered flow to formulate practical relations for the mixing length, hence they are not general. Secondly, they prescribe that turbulent diffusivities be zero where there is no velocity gradient, as it happens for the centerline of mini/micro channels, although this clashes with the experimental evidence [19]. Concerning variable physical properties, the previous models substantially adopt common correlations by reducing the problem to calculate a modified y^+, but it should be better to consider differential equations. Finally, only the model of Bellmore and Reid considers the density fluctuations, but it requires the average absolute deviations, which are not accessible by most widespread turbulence models. Moreover, Eq. (31), which has been deduced according to the generalized decomposition given by Eq. (30), is in contrast with the gradient-diffusion hypothesis because it depends on the radial enthalpy gradient instead of the axial one as expected because it involves the axial velocity component.

A different approach is proposed. Within the framework of the mixing length theory, the turbulence closure model can be considered a tool which allows us to calculate robust correlation coefficients $C_{uv} = l^2_{\mathrm{m}}/(l_u l_v)$ and $C_{hv} = l^2_{\mathrm{m}}/(Pr_{\mathrm{t}} l^2_v)$. Analogously, when Eq. (31) is considered, the general decomposition reduces to suppose $C_{hu} = C_{hv}l_v/l_u$. The coefficients b_i involved in factorized heuristic assumptions given by Eqs. (28) and (29) can be expressed as functions of second-order mixed robust correlation coefficients C_{hv}, C_{hu} and C_{uv}, which are the non-zero lowest-order coefficients. Substituting these expressions into Eq. (30), a modified expression is found

$$\langle(u')^{n_1}(v')^{n_2}(h')^{n_3}\rangle = (-\zeta)^{n_3}C^{q_1}_{hv}C^{q_2}_{hu}C^{q_3}_{uv}\langle|u'|\rangle^{n_1}\langle|v'|\rangle^{n_2}\langle|h'|\rangle^{n_3}, \quad (34)$$

where $q_i \in \mathbb{Q}$ is defined as $q_i = \sum_{j=1}^{3}(1 - 2\delta_{ij})n_j/2$ and δ_{ij} is the Kronecker operator. Mathematically, the general decomposition given by Eq. (30) is equivalent to suppose that higher-order robust correlation coefficients are proper combinations of lower-order ones. Since, by definition $n_i = \sum_{j=1}^{3}(1 - \delta_{ij})q_j$ and recalling the expressions for lower-order correlation coefficients given by Eqs. (28), (29) and (31), the previous decomposition can be modified as

$$\langle(u')^{n_1}(v')^{n_2}(h')^{n_3}\rangle = (-\zeta)^{n_3}|\langle h'v'\rangle|^{q_1}|\langle h'u'\rangle|^{q_2}\langle u'v'\rangle^{q_3}. \quad (35)$$

This correlation has been rigorously demonstrated within the framework of the theory developed by Bellmore and Reid and so it can be considered equivalent to the decomposition given by Eq. (30). The main advantage is that it involves only quantities that are calculated by all turbulence closure models because they emerge from time averaging of flow equations with constant properties. Essentially the previous relation can be considered as a constitutive hypothesis assuming that terms due to density fluctuations depend on usual terms due to velocity fluctuations. In the following, the turbulent viscosity hypothesis given by Eq. (9) and the gradient-diffusion hypothesis given by Eq. (10) will be considered in order to produce a meaningful example without loss of generality. Applying Eq. (35) to all turbulent terms involved into Eqs. (22) and (23), we find again the same formal expression for the corrective factor ϕ which influences effective diffusivities given by Eq. (32), but with a different intensity index σ, given by

$$\sigma = \sqrt{\frac{\lambda^2_{\mathrm{t}}}{\bar{\rho}\mu_{\mathrm{t}}}\frac{|\partial_x T\partial_r T|}{|\partial_r\bar{u}|}}. \quad (36)$$

We can proceed in the same way for the characteristic velocity, obtaining

$$\bar{u}^* = \zeta\beta(\lambda_t/\bar{\rho})|\partial_x T| \ll \bar{v}^* = \zeta\beta(\lambda_t/\bar{\rho})|\partial_r T|. \quad (37)$$

Since these relations involve the temperature gradient, contrarily to previous ones which involve enthalpy gradient, the effects due to compressibility must be discussed. For both axial and radial direction, the generic component of the enthalpy gradient can be expressed by means of temperature and pressure changes $\partial_i \bar{h} = c_p T[\partial_i T/T - \varphi \partial_i p/p]$, where c_p is the specific heat capacity $c_p = \partial_T \bar{h}|_p$ and the dimensionless parameter φ takes into account non-ideal gas effects, namely $\varphi = (\beta c_p T - 1)/(\bar{\rho} c_p T/p)$. In all the following calculations, this parameter is included over the range $0 < \varphi < 0.21$. Since the relative temperature changes are much greater than relative pressure changes $\partial_i T/T \gg \partial_i p/p$, then the compressibility effects on enthalpy can be neglected and an approximate relation yields $\partial_i \bar{h} \approx c_p \partial_i T$. For comparing the previous results with those obtained by Bellmore and Reid, Eqs. (32) and (33) will be directly generalized by expressing mixing length and turbulent Prandtl number as functions of turbulent diffusivities. Recalling that $l_m = \mu_t^{1/2}(\rho|\partial_r \bar{u}|)^{-1/2}$ and $Pr_t = \mu_t|\partial_r \bar{h}|(\lambda_t|\partial_r T|)^{-1}$, the generalized expressions for the intensity index and for the components of characteristic velocity become

$$\sigma_{BR} = \sqrt{\frac{\lambda_t^2}{\bar{\rho}\mu_t}\frac{|\partial_r T|^2}{|\partial_r \bar{u}|}}, \quad (38)$$

$$\bar{u}^*_{BR} = \bar{v}^*_{BR} = \zeta\beta(\lambda_t/\bar{\rho})|\partial_r T|. \quad (39)$$

Despite the simplicity of the procedure, Eqs. (38) and (39) can be calculated by any turbulence model too. In this second case, the intensity index σ_{BR} depends only on radial temperature gradient, while the intensity index σ calculated by the proposed approach depends on the temperature gradient along both directions. If density fluctuations are due to enthalpy fluctuations and the latter ones satisfy the gradient-diffusion hypothesis by given Eq. (10), which is strongly anisotropic, it is not clear why the effects due to density fluctuations should be isotropic. Since the original formulation of Bellmore and Reid was developed for boundary layer flow, the generalized Eqs. (38) and (39) overestimate the effect of axial density fluctuations and they are not universally valid. Here an essential feature of the proposed model emerges. Eqs. (36) and (37) involve the axial gradient to predict the effects due to density fluctuations along the axial direction. This feature essentially predicts a lower effect of density fluctuations on turbulent diffusivities since $\sigma \ll \sigma_{BR}$, because usually $|\partial_x T| \ll |\partial_r T|$. Concerning the effects on convective terms, the two formulations are formally equivalent for the radial direction $\bar{v}^* = \bar{v}^*_{BR}$, while they again differ for the axial direction $\bar{u}^* \ll \bar{u}^*_{BR}$. Since the latter effect is negligible in the considered application, the essential difference between the two approaches for simulation of mini/micro channels lies in the description of the effective diffusivities and, in particular, in the fact that $|\phi - 1| \ll |\phi_{BR} - 1|$.

Any turbulence closure model can be applied to calculate turbulent diffusivities into Eqs. (36) and (37). In the following, two 2-equation models will be considered in order to compare the effects due to the description of turbulent diffusivities. The additional terms due to fluctuating properties within these equations can be neglected as a first approximation, in order to reduce the computational resources. The numerical results confirm this approximation because there is a reasonable match with experimental data or, at least, the experimental data are not so accurate to properly discriminate the effects of this approximation. In particular, the standard k–ϵ model [26] and the RNG k–ϵ model [28] were considered. Since both 2-equation models were formulated for fully-developed turbulence, they are not usually applied in the near-wall region (approximately $0 < y^+ < 60$), where 1-equation model will be adopted [27].

At the inlet boundary, some unknown quantities, which describe the fluid flow, are supposed uniformly distributed along the radial direction: $\bar{u}(0,r) = u_0$, $\bar{v}(0,r) = 0$ and $T(0,r) = T_0$. At the outlet boundary, the only calculation unknown which was not considered within inlet conditions, i.e. pressure, is imposed $p(L) = p_L$. At the wall boundary, a given thermal flux $\partial_r T = q_w/\lambda$ or, alternatively, a given wall temperature $T(x,R) = T_w$ is considered, while the velocity components are set as $\bar{u}(x,R) = 0$ and $\bar{v}(x,R) = 0$. It is possible to proceed in a very similar way for turbulent quantities involved into 2-equation models [27].

3. Numerical discretization and solution procedure

The governing equations of continuity (13), momentum (14) and energy (15) conservation were discretized, according to the finite volume method [35,36]. The general upwind scheme was adopted to calculate the convective terms for all linearized equations [36].

Since for short mini/micro channels pressure drops are negligible, the thermophysical properties can be considered as functions of temperature only. Piecewise linear approximations of the thermophysical properties, given by the considered database [34], will be adopted and the distribution of nodal values will be properly chosen for ensuring the desired accuracy. In the following calculations, the error thresholds are 0.3–5.6% for heat capacity, 0.1–2% for thermal conductivity, 0.1–0.5% for modified compressibility and 0.1–0.5% for both density and dynamic viscosity.

An axially homogeneous mesh and a characteristic length of the generic control volume Δx comparable to the radial dimension was adopted. On the other hand,

the radial discretization of the computational domain should be very fine near the wall in order to solve the equations over the laminar viscous sublayer ($y^+ < 5$). Usually the thickness of the control volume adjacent to the wall Δr_w is determined such that the dimensionless distance y_w^+ of the centroid is approximately equal to one [37]. This practice allows us to estimate the thickness of the control volume adjacent to the wall as Δr_w^+. Radially homogeneous meshes would enormously increase the computational time. For this reason, the thickness of the control volume adjacent to the axis of the mini/micro channel Δr_a is assumed much greater than previous one $\Delta r_a \gg \Delta r_w$. A geometric progression with ratio $\chi = (R - \Delta r_a)/(R - \Delta r_w)$ can be assumed to properly blend the previous extremes.

For turbulent convective heat transfer at supercritical pressure near the critical point, the condition $y_w^+ \approx 1$ is not the only one and is not the most severe. Since the easiest way to approximate the solution between two consecutive nodal values is to consider a linear function [36], an error could occur in estimating the physical properties if too coarse meshes are considered. If very high-density meshes are avoided [7], only a local grid refinement can mitigate this problem [35]. The basic idea is to guarantee that the temperature difference between two adjacent control volumes is small enough to produce acceptable errors in estimating the maximum specific heat capacity. In this case, the limiting radial discretization in the buffer region due to the pseudo-critical temperature is much more severe than that given by low-Reynolds turbulence models: in particular, $\Delta r_c/\Delta r_w^+ < 0.18$ for the reported calculations.

The greatest mesh used in the numerical simulations reported further on is characterized by 118 radial nodes, which are much less than those prescribed by single-progression high-density meshes [7]. However this radial discretization step and a proper local grid refinement enables one to produce mesh independent results and numerical errors comparable with the accuracy of the thermophysical database.

The discretized governing equations for continuity, momentum and energy are solved sequentially by SIMPLE algorithm [27]. The relative convergence criterion is equal to 1×10^{-3} for the validation cases [37], which are characterized by fixed wall thermal flux, and it is equal to 1×10^{-5} for the experimental runs, which are characterized by fixed wall temperature. For each discretized equation, a Gauss–Seidel linear equation solver is used in conjunction with an algebraic multi-grid method to solve the resulting scalar system of equations for the solving variables [27]. In order to prevent divergence, the velocity components in the momentum equations, the temperature in the energy equation and the transport properties are updated by corrective quantities smaller than those due to pure calculation. Near the critical point, Lee and Howell [37] suggested to iteratively renew with an under-relaxation factor the thermophysical properties too. This practice realizes a multi-level under-relaxation which prevents strong instabilities emerging when too coarse meshes are adopted to describe fluid flow near the critical point. If the mesh is chosen according to previously discussed strategy, there is no need for multi-level under-relaxation.

4. Results and discussion

4.1. Comparison with other predictions and experimental data for the local heat transfer coefficient

The comparison with experimental measurements of local heat transfer coefficients is meaningful for verifying the reliability of the numerical results. Due to experimental difficulties, there have been few radial temperature measurements inside a tube which involve the pseudo-critical temperature. The experimental data for a normal sized duct due to Wood and Smith [38] will be considered. They considered an upward flow of carbon dioxide under heating conditions in a tube with common diameter ($d = 22.91$ mm) and measured radial temperature profiles by keeping the wall thermal flux fixed. The same set of data has been considered for validation purposes by Lee and Howell [37]. In this case, the effect of gravity has been added to the momentum equation, since Eq. (1) did not hold for this case.

In Fig. 1 the effect of the radial discretization on the solution is reported. The mesh based on low Reynolds-number models shows to be too coarse for describing

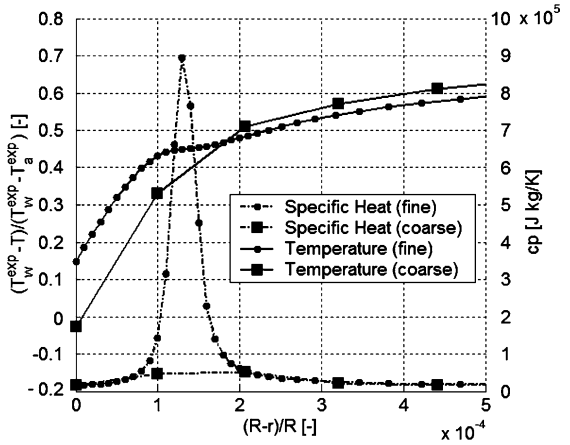

Fig. 1. Effect of radial discretization on the solution. The predicted profiles for specific heat capacity and fluid temperature are both reported in a thin layer near the wall. Both meshes are based on geometric progression. The coarse mesh, which realizes $y_w^+ \approx 1$, is not suitable to describe the peak in specific heat. The reported markers are representative of grid nodes.

the peak of specific heat capacity and, consequently, to produce misleading conclusions. In fact, the coarse mesh could lead one to think that the model of Bellmore and Reid works better than it really does. The coarse mesh shows a strong unstable behavior because the solution process tries to cut off the peak in specific heat capacity, which behaves like local numerical noise breaking the smooth solution. This probably justifies the need of multi-level under-relaxation in the numerical simulations performed by Lee and Howell [37].

A comparison of predicted profiles of dimensionless temperature calculated by means of different models with experimental data by Wood and Smith [38] in a thin layer near the wall is shown in Fig. 2. The reported cases are different because of the wall thermal flux, which is 63.05 kW/m^2 for *Test A* and 204.91 kW/m^2 for *Test B*. Because of the high mass flow rate ($Re = 9.3 \times 10^5$), the pseudo-critical temperature is positioned near the wall and it is well confined within a small buffer region. In both tests the model of Bellmore and Reid underestimates the wall temperature $T_w < T_w^{exp}$. This result partially contradicts the conclusion of Lee and Howell [37], which was probably due to the previously discussed effects of coarse discretization. The proposed approach for taking into account the effects of density fluctuations has been applied together with both the standard k–ϵ model and the RNG k–ϵ model. In both tests, the standard k–ϵ model overestimates the wall temperature

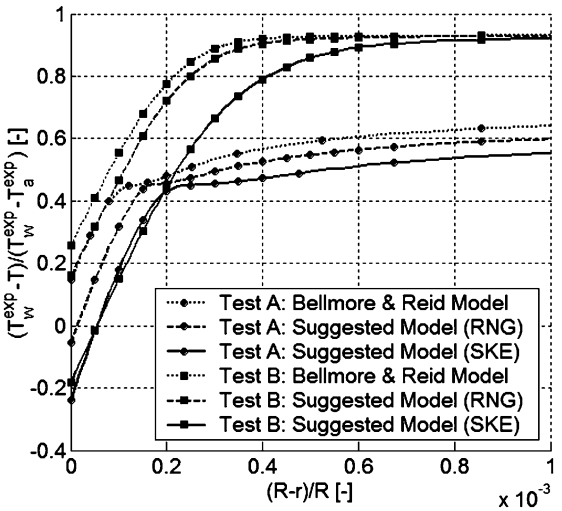

Fig. 2. Comparison of predicted profiles of dimensionless temperature calculated by means of different models with experimental data of Wood and Smith [38] in a thin layer near the wall. The reported cases are different because of the wall thermal flux, which is 63.05 kW/m^2 for *Test A* and 204.91 kW/m^2 for *Test B*. The label "RNG" means RNG k–ϵ model and the label "SKE" means standard k–ϵ model. The reported markers are not representative of grid nodes.

$T_w > T_w^{exp}$ and the RNG k–ϵ model produces the best results. The proposed approach allows formulating numerical predictions of wall temperature which differ from experimental data by ±20% (see Table 1).

The whole radial temperature profiles are reported into Fig. 3. Also in this case, the numerical predictions due to the proposed approach are in good agreement with the experimental data. In both tests, the standard k–ϵ model better reproduces the dimensionless temperature profile in the bulk region, while RNG k–ϵ model better reproduces the wall temperature. For this reason, in the next section both models will be considered.

4.2. Comparison with other predictions and experimental data for average heat transfer coefficient

In this section, the numerical results will be compared with some phenomenological correlations for estimating the average heat transfer coefficients. In all these calculations, the effects due to the gravity field have been purposely excluded in order to verify if buoyancy is responsible for heat transfer impairment.

The operating conditions of the numerical simulations were selected according to a proper design of experiments [39]. For the present application, there are five factors usually considered by all phenomenological correlations: the working pressure p; the bulk temperature $T_b(x)$; the wall temperature $T_w(x)$; the diameter of mini/micro channel d and finally the mass flow rate, G. In the experimental runs, the wall temperature $T_w(x) = T_w$ will be assumed uniformly distributed along the axial direction and the final goal will be the calculation of the wall thermal flux $q_w(x)$. The turbulence model M completes the set of factors. The response is given by the average heat transfer coefficient. In the present work, the following definition will be adopted

$$\alpha_L = \frac{\left(\int_0^L q_w \, dx\right) \Big/ L}{(\theta_0 - \theta_L)/\ln(\theta_0/\theta_L)}, \tag{40}$$

where $\theta_0 = T_b(0) - T_w$ and $\theta_L = T_b(L) - T_w$.

The main trends of the response was investigated by means of a finite number of levels. Concerning the pressure, a slightly supercritical pressure and a much higher pressure are considered. Concerning the bulk temperature, the levels should allows us to investigate the effects of pseudo-critical temperature. Let us consider the following function defined as

$$c_p^w(T) = \frac{1}{T - T_w} \int_{T_w}^{T} \bar{h}(T, p) \, dT. \tag{41}$$

The previous quantity allows us to define the specific heat capacity at the wall $c_p^{ww} = \lim_{T \to T_w} c_p^w(T)$ and the average specific heat capacity $c_p^{wb} = c_p^w(T_b)$. Many authors agree on the importance of the ratio c_p^{wb}/c_p^{ww} between the average and the wall specific heat capacity to

Table 1
Comparison among numerical predictions of local heat transfer coefficients, experimental data of Wood and Smith [38] (label "W&S") and other numerical predictions of Lee and Howell [37] (label "L&H")

Parameters	W&S (Exp.)	L&H (B&R)	This work (B&R)	This work (RNG)	This work (SKE)
Test A: $q_w = 63.05\ kW/m^2$, $T_b = 302.82\ K$, $Re = 9.3 \times 10^5$					
T_w (K)	305.76	305.60	305.29	305.94	306.51
α (kW/m^2 K)	21.45	23.88	25.53	20.21	17.09
e_α (%)	0	+11.3	+19.0	**−5.8**	−20.3
Test B: $q_w = 204.91\ kW/m^2$, $T_b = 303.15\ K$, $Re = 9.3 \times 10^5$					
T_w (K)	327.37	323.20	320.97	323.38	331.88
α (kW/m^2 K)	8.46	10.62	11.50	10.13	7.13
e_α (%)	0	+25.5	+35.9	+19.7	**−15.7**

The considered models are: the model of Bellmore and Reid [24] (label "B&R"); the RNG k–ϵ model (label "RNG") and the standard k–ϵ model (label "SKE"). The best results are bold-faced.

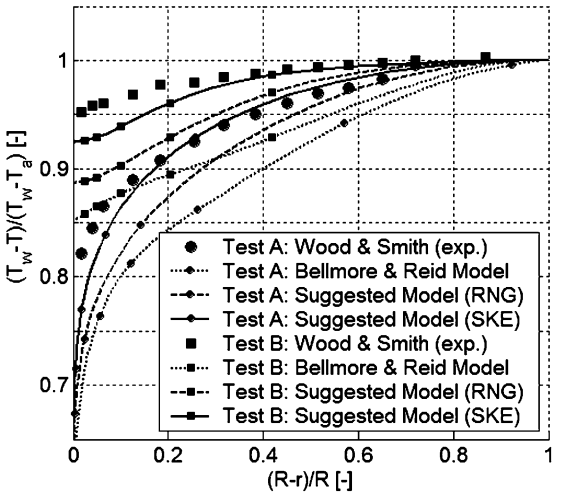

Fig. 3. Comparison of predicted profiles of dimensionless temperature calculated by means of different models with experimental data of Wood and Smith [38] at a given axial location. The reported cases differ are different because of the wall thermal flux, which is 63.05 kW/m^2 for *Test A* and 204.91 kW/m^2 for *Test B*. The label "RNG" means RNG k–ϵ model and the label "SKE" means standard k–ϵ model. The reported markers are not representative of grid nodes.

characterize heat transfer near the critical point [9,13,15]. The ratio c_p^{wb}/c_p^{ww} discriminates the cases characterized by $T_b(x) \approx T_{pc}$, which implies $c_p^{wb} > c_p^{ww}$, and the other case characterized by $T_w(x) \approx T_{pc}$, which implies $c_p^{wb} < c_p^{ww}$. The factorial design must take into account both configurations, too. Three inlet bulk temperatures are selected: the first very close to the pseudo-critical value $T_0 \approx T_{pc}$; the second, higher than previous one, so that the wall temperature can be close to the pseudo-critical value $T_w \approx T_{pc}$ and the third much higher. Concerning wall temperature, the difference $T_0 - T_w$ is increased far from the pseudo-critical temperature where heat transfer is weaker. Since the effects due to gravity field are neglected, Eq. (1) allows us to reduce the number of free parameters. The buoyancy parameter can be factorized $Gr/Re_0^2 = Bo_T Bo_G$, where

$$Bo_T = \frac{\rho_w \rho_0 - \rho_0^2}{\rho_{pc}^2}, \tag{42}$$

$$Bo_G = \frac{\pi^2}{16} \frac{g \rho_{pc}^2 d^5}{G^2}. \tag{43}$$

Since the selected factorial design implies $Bo_T \leqslant 6.09 \times 10^{-1}$, Eq. (1) reduces to $Bo_G \leqslant 1.64 \times 10^{-3}$. In the following $Bo_G = 1.31 \times 10^{-3}$ is assumed and two levels for the mini/micro channel diameter ($d < 2$ mm), or equivalently two levels for the mass flow rate, are selected. Finally, three turbulence models are included: the approach of Bellmore and Reid and the proposed approach, together with both the RNG k–ϵ model and the standard k–ϵ model. The previous assumptions define a simplified $2 \times 3 \times 2 \times 2 \times 3$ factorial design [39], which requires 72 runs.

In Tables 2–5 the numerical predictions of the average heat transfer coefficient α_L for the experimental runs are reported. Concerning the turbulence modeling, the standard k–ϵ model systematically produces lower values for the average heat transfer coefficient in comparison with the RNG k–ϵ model. In the previous section, the fact that the standard k–ϵ model overestimates the effective temperature difference $|T_b - T_w|$ has been already pointed out and it is consistent with the present results. Usually the average heat transfer coefficients predicted by the RNG k–ϵ model are slightly lower than those due to the model of Bellmore and Reid, with the exception of the experimental runs which are characterized by $T_0 \approx T_{pc}$ and which reveal a reverse trend. When the pseudo-critical temperature is close to bulk temperature, the radial temperature profile looks similar to a step function and the RNG k–ϵ model allows us to properly describe this strained flow. Concerning the inlet temperature difference $|T_0 - T_w|$, the location of the pseudo-critical temperature plays an important part.

Table 2
Numerical predictions of average heat transfer coefficient α_L for experimental runs 1–18 defined by the factorial design

	Factorial design						Results		
	p (MPa)	T_0 (K)	T_w (K)	d (mm)	G (g/s)	M	q_w (kW/m^2)	$\lvert\Delta T_b\rvert$ (K)	α_L (kW/m^{2}K)
1	7.412	305	302	0.787	0.571	B&R	111.92	0.69	42.359
2	7.412	305	302	0.787	0.571	RNG	115.57	0.69	43.803
3	7.412	305	302	0.787	0.571	SKE	99.38	0.67	37.519
4	7.412	305	298	0.787	0.571	B&R	172.60	1.97	28.955
5	7.412	305	298	0.787	0.571	RNG	176.55	2.19	30.244
6	7.412	305	298	0.787	0.571	SKE	159.10	1.38	25.307
7	7.412	312	309	0.787	0.571	B&R	18.71	2.33	12.004
8	7.412	312	309	0.787	0.571	RNG	17.52	2.19	10.484
9	7.412	312	309	0.787	0.571	SKE	15.91	2.01	8.772
10	7.412	312	305	0.787	0.571	B&R	58.35	5.65	16.991
11	7.412	312	305	0.787	0.571	RNG	54.49	5.41	14.972
12	7.412	312	305	0.787	0.571	SKE	48.65	5.02	12.236
13	7.412	360	353	0.787	0.571	B&R	17.55	6.01	5.704
14	7.412	360	353	0.787	0.571	RNG	16.76	5.74	5.013
15	7.412	360	353	0.787	0.571	SKE	15.87	5.44	4.383
16	7.412	360	340	0.787	0.571	B&R	50.23	16.56	5.344
17	7.412	360	340	0.787	0.571	RNG	49.86	16.47	5.243
18	7.412	360	340	0.787	0.571	SKE	47.12	15.60	4.575

The lowest supercritical pressure (7.412 MPa) and the smallest mini/micro channel diameter (0.787 mm) are considered. The adopted models are: the model of Bellmore and Reid [24] (label "B&R"); the RNG k–ϵ model (label "RNG") and the standard k–ϵ model (label "SKE"). The pseudo-critical temperature is T_{pc} = 304.328 K.

The experimental runs #4 and #10 (see Table 2) share the same inlet temperature difference $|T_0 - T_w| = 7$ K but for the first run $T_b(0) \approx T_{pc}$, which implies $c_p^{wb}/c_p^{ww} = 3.94$, while for the second run $T_w \approx T_{pc}$, which implies $c_p^{wb}/c_p^{ww} = 0.35$. The effect on the average heat transfer coefficient is impressive: $\alpha_L = 28.96$ kW/m^{2}K for the experimental run #4 and $\alpha_L = 16.99$ kW/m^{2}K for the experimental run #10. This confirms the common practice to include the ratio c_p^{wb}/c_p^{ww} in the phenomenological correlations and to assign it a positive exponent interpolating the experimental data. Concerning the diameter of the mini/micro channel, or equivalently the mass flow rate, the factorial design is based on the assumption to keep the parameter Bo_G, given by Eq. (43), fixed so as to satisfy the threshold which allows us to neglect the buoyancy effects. This means that G^2/d^5 is constant and then the inlet bulk velocity $u_0 \propto G/d^2 \propto d^{1/2}$ modestly increases by doubling the diameter of mini/micro channel. Concerning the supercritical pressure, the peak of the specific heat capacity at the pseudo-critical temperature enhances the convective heat transfer and the enhancement is proportional to the magnitude of the peak. The experimental runs #19 (see Table 3) and #55 (see Table 5) are both characterized by $T_b(0) \approx T_{pc}$, so that $c_p^{wb}/c_p^{ww} > 1$. The effective temperature difference for the first experimental run $|T_0 - T_w| = 3$ K is smaller than the one for the second experimental run $|T_0 - T_w| = 10$ K. In spite of this, the predicted wall thermal fluxes are comparable: $q_w = 131.5$ kW/m^2 for the experimental run #19 and $q_w = 103.21$ kW/m^2 for the experimental run #55. The lowest supercritical pressure, considered by the first experimental run, causes the specific heat capacity to strongly change in the radial direction ($c_p^{wb}/c_p^{ww} = 4.62$) while the highest supercritical pressure is much less effective in doing the same ($c_p^{wb}/c_p^{ww} = 1.17$).

In Table 6 the numerical results are compared with other numerical predictions and some phenomenological correlations. The correlation proposed by Petrov and Popov [10] is included within the numerical results, because it was developed by interpolation of some numerical simulations. At least for the selected factorial design, the proposed approach reasonably reproduces both results due to Petrov and Popov and results due to the model of Bellmore and Reid, if the standard k–ϵ model and the RNG k–ϵ model are assumed respectively. This means that the proposed approach is general enough to reproduce different models independently developed.

In Table 6, the experimental correlations due to Liao and Zhao [13], Pettersen et al. [11], Pitla et al. [12] and Yoon et al. [15] are considered too. The first correlation was specifically developed for a single mini/micro channel. The second one derives from some experimental tests on a flat extruded tube, which involves many

Table 3
Numerical predictions of average heat transfer coefficient α_L for experimental runs 19–36 defined by the factorial design

	Factorial design						Results		
	p (MPa)	T_0 (K)	T_w (K)	d (mm)	G (g/s)	M	q_w (kW/m^2)	$\lvert\Delta T_b\rvert$ (K)	α_L (kW/m^{2}K)
19	7.412	305	302	1.417	2.482	B&R	131.49	0.63	49.242
20	7.412	305	302	1.417	2.482	RNG	162.26	0.66	61.020
21	7.412	305	302	1.417	2.482	SKE	134.35	0.64	50.341
22	7.412	305	298	1.417	2.482	B&R	231.75	0.67	34.806
23	7.412	305	298	1.417	2.482	RNG	280.40	0.70	42.188
24	7.412	305	298	1.417	2.482	SKE	239.90	0.67	36.035
25	7.412	312	309	1.417	2.482	B&R	26.47	1.43	11.968
26	7.412	312	309	1.417	2.482	RNG	26.22	1.41	11.813
27	7.412	312	309	1.417	2.482	SKE	22.94	1.22	9.875
28	7.412	312	305	1.417	2.482	B&R	79.42	3.75	16.256
29	7.412	312	305	1.417	2.482	RNG	80.34	3.79	16.522
30	7.412	312	305	1.417	2.482	SKE	69.42	3.67	13.521
31	7.412	360	353	1.417	2.482	B&R	27.84	3.98	5.879
32	7.412	360	353	1.417	2.482	RNG	26.89	3.85	5.574
33	7.412	360	353	1.417	2.482	SKE	24.43	3.50	4.838
34	7.412	360	340	1.417	2.482	B&R	82.92	11.54	6.183
35	7.412	360	340	1.417	2.482	RNG	79.99	11.15	5.850
36	7.412	360	340	1.417	2.482	SKE	72.80	10.18	5.088

The lowest supercritical pressure (7.412 MPa) and the biggest mini/micro channel diameter (1.417 mm) are considered. The adopted models are: the model of Bellmore and Reid [24] (label "B&R"); the RNG k–ϵ model (label "RNG") and the standard k–ϵ model (label "SKE"). The pseudo-critical temperature is T_{pc} = 304.328 K.

Table 4
Numerical predictions of average heat transfer coefficient α_L for experimental runs 37–54 defined by the factorial design

	Factorial design						Results		
	p (MPa)	T_0 (K)	T_w (K)	d (mm)	G (g/s)	M	q_w (kW/m^2)	$\lvert\Delta T_b\rvert$ (K)	α_L (kW/m^{2}K)
37	12.000	327	317	0.787	0.571	B&R	67.21	6.78	11.232
38	12.000	327	317	0.787	0.571	RNG	70.36	7.13	12.322
39	12.000	327	317	0.787	0.571	SKE	64.91	6.53	10.518
40	12.000	327	307	0.787	0.571	B&R	133.53	15.18	12.519
41	12.000	327	307	0.787	0.571	RNG	132.12	14.98	12.189
42	12.000	327	307	0.787	0.571	SKE	123.04	13.70	10.374
43	12.000	347	337	0.787	0.571	B&R	52.14	8.08	10.658
44	12.000	347	337	0.787	0.571	RNG	49.65	7.75	9.549
45	12.000	347	337	0.787	0.571	SKE	45.76	7.21	8.097
46	12.000	347	327	0.787	0.571	B&R	112.99	15.24	10.641
47	12.000	347	327	0.787	0.571	RNG	118.00	15.75	11.606
48	12.000	347	327	0.787	0.571	SKE	108.26	14.75	9.815
49	12.000	360	353	0.787	0.571	B&R	25.11	5.54	7.101
50	12.000	360	353	0.787	0.571	RNG	25.22	5.56	7.176
51	12.000	360	353	0.787	0.571	SKE	23.58	5.22	6.181
52	12.000	360	340	0.787	0.571	B&R	81.61	16.01	8.214
53	12.000	360	340	0.787	0.571	RNG	82.68	16.18	8.460
54	12.000	360	340	0.787	0.571	SKE	76.88	15.23	7.237

The highest supercritical pressure (12.0 MPa) and the smallest mini/micro channel diameter (0.787 mm) are considered. The adopted models are: the model of Bellmore and Reid [24] (label "B&R"); the RNG k–ϵ model (label "RNG") and the standard k–ϵ model (label "SKE"). The pseudo-critical temperature is T_{pc} = 327.1 K.

Table 5
Numerical predictions of average heat transfer coefficient α_L for experimental runs 55–72 defined by the factorial design

	Factorial design						Results		
	p (MPa)	T_0 (K)	T_w (K)	d (mm)	G (g/s)	M	q_w (kW/m^2)	$\lvert\Delta T_b\rvert$ (K)	α_L (kW/m^{2}K)
55	12.000	327	317	1.417	2.482	B&R	103.21	4.18	13.367
56	12.000	327	317	1.417	2.482	RNG	109.08	4.43	14.411
57	12.000	327	317	1.417	2.482	SKE	95.39	3.85	12.048
58	12.000	327	307	1.417	2.482	B&R	219.42	9.52	14.898
59	12.000	327	307	1.417	2.482	RNG	213.88	9.25	14.354
60	12.000	327	307	1.417	2.482	SKE	189.73	8.07	12.147
61	12.000	347	337	1.417	2.482	B&R	84.63	5.67	12.489
62	12.000	347	337	1.417	2.482	RNG	76.78	5.18	10.821
63	12.000	347	337	1.417	2.482	SKE	67.98	4.63	9.128
64	12.000	347	327	1.417	2.482	B&R	177.25	10.18	12.753
65	12.000	347	327	1.417	2.482	RNG	184.83	11.20	13.545
66	12.000	347	327	1.417	2.482	SKE	162.97	10.09	11.340
67	12.000	360	353	1.417	2.482	B&R	43.97	4.07	9.410
68	12.000	360	353	1.417	2.482	RNG	39.62	3.68	8.033
69	12.000	360	353	1.417	2.482	SKE	35.58	3.32	6.890
70	12.000	360	340	1.417	2.482	B&R	130.84	11.27	9.622
71	12.000	360	340	1.417	2.482	RNG	130.56	11.25	9.592
72	12.000	360	340	1.417	2.482	SKE	116.80	10.18	8.162

The highest supercritical pressure (12.0 MPa) and the biggest mini/micro channel diameter (1.417 mm) are considered. The adopted models are: the model of Bellmore and Reid [24] (label "B&R"); the RNG k–ϵ model (label "RNG") and the standard k–ϵ model (label "SKE"). The pseudo-critical temperature is $T_{pc} = 327.1$ K.

Table 6
Comparison among numerical predictions for average heat transfer coefficients, some phenomenological correlations [13,11,12,15] and other numerical predictions [10]

Experimental correlations	Numerical predictions			
	Mean ± standard deviation $e_\alpha^L = (\alpha_L - \alpha_L^{exp})/\alpha_L^{exp}$ (%)			
	Petrov & Popov correlation	This work		
		B&R	RNG	SKE
Liao & Zhao	50.6 ± 34.6	79.1 ± 48.3	49.7 ± 34.8	76.2 ± 39.2
Pettersen et al.	6.7 ± 25.4	25.9 ± 27.1	5.1 ± 18.6	24.1 ± 23.3
Pitla et al.	8.0 ± 36.1	25.5 ± 23.7	6.3 ± 25.9	25.4 ± 31.7
Yoon et al.	−37.6 ± 6.2	−25.8 ± 11.8	−37.9 ± 6.2	−26.8 ± 7.4

The considered models are: the model of Bellmore and Reid [24] (label "B&R"); the RNG k–ϵ model (label "RNG") and the standard k–ϵ model (label "SKE").

mini/micro channels along axial directions. The correlation of Pitla et al. improves the previous one by averaging the results obtained with constant properties evaluated at the wall and bulk temperature. Unfortunately this practice shifts the peak of the average heat transfer coefficient from the pseudo-critical temperature and it is not consistent with any theoretical explanation. Finally the correlation of Yoon et al. has been recently developed for normal-sized ducts.

First of all, the numerical results seem to show that the buoyancy effects are not completely responsible for heat transfer impairment measured by Liao and Zhao for mini/micro channels. Despite the fact that the gravity field is completely neglected by numerical simulations, the final predictions systematically overestimate the results due to the correlation of Liao and Zhao. If the experimental data are reliable, some additional terms must be included into the model to justify the heat transfer impairment for mini/micro channels. Secondly, if a preference among phenomenological correlations on the basis of numerical results is needed, the results due to the RNG k–ϵ model and the standard k–ϵ model can be grouped together, as reported in Fig. 4. The grouped results express a moderate preference for the

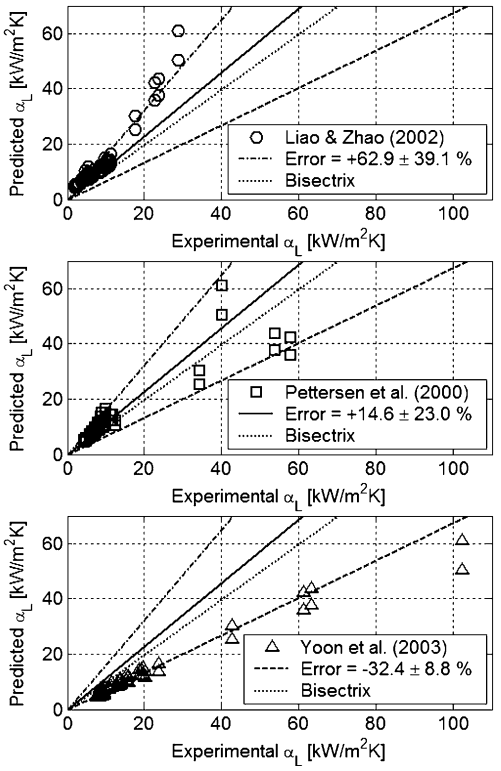

Fig. 4. The average heat transfer coefficients obtained by both the RNG k–ϵ model and the standard k–ϵ model are jointly reported, in order to duplicate the predictions for the same run. Some phenomenological correlations are considered [13,11,15]. For each subplot, the numerical error due to comparison with a phenomenological correlation is reported too, in terms of mean value and standard deviation.

correlation proposed by Pettersen et al. [11]. This result is not conclusive because the experimental measurements for a single mini/micro channels should be more reliable than the measurements for a flat extruded tube. Anyway some numerical predictions show that the transverse non-homogeneities for a flat extruded tube are much more smaller than it could have been initially supposed [40].

Some concluding remarks on additional turbulent terms due to time averaging of density fluctuations are discussed. In Fig. 5 the corrective factor for turbulent diffusivities due to density fluctuations is reported. According to the assumed boundary conditions, the transverse sections of a mini/micro channel closer to the inlet are characterized by stronger radial temperature gradients. This means they have higher indexes of intensity for density fluctuations σ_{BR} and consequently more effective corrective factors for turbulent diffusivities ϕ_{BR}. Nevertheless, the maximum correction reported in Fig. 5 is less than 3%. This threshold is even smaller for the proposed approach because $|\phi - 1| \ll$

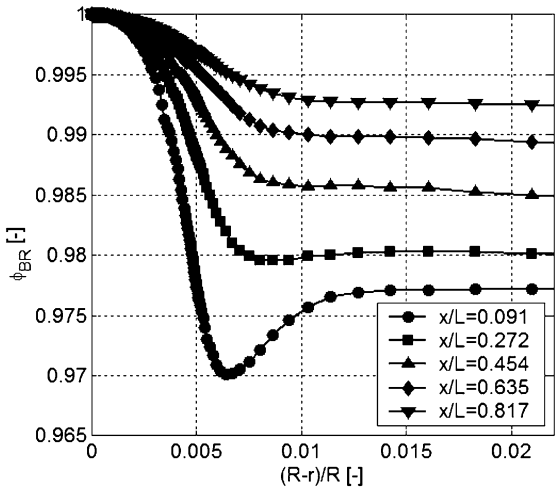

Fig. 5. Radial profile of the corrective factor for turbulent diffusivities due to density fluctuations in a thin layer near the wall, according to the model of Bellmore and Reid [24]. Cooling conditions are considered. The reported markers are representative of grid nodes.

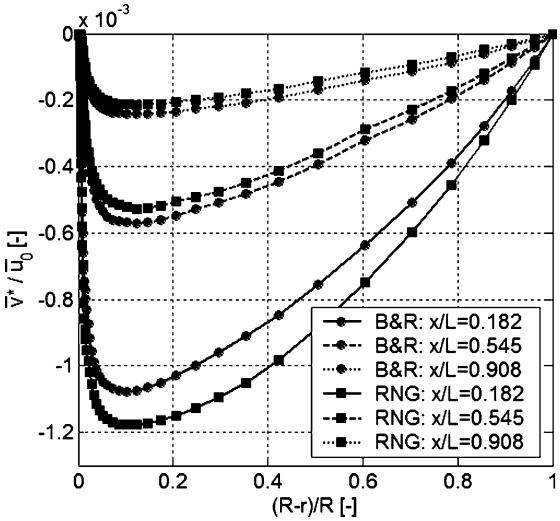

Fig. 6. Normalized radial component of the characteristic velocity for density fluctuations at the same locations, according to different models. The model of Bellmore and Reid (label "B&R") and the suggested approach together with RNG k–ϵ model (label "RNG") are considered. The reported markers are representative of grid nodes.

$|\phi_{\mathrm{BR}} - 1|$, as previously discussed. In Fig. 6 some results are reported for radial component of the characteristic velocity for density fluctuations, according to different models. The formal expression of the radial component of the characteristic velocity for both models is the same $\bar{v}^* = \bar{v}^*_{\mathrm{BR}}$, as it can be easily verified by considering Eqs. (37) and (39). An estimation of the axial component of

the characteristic velocity can be obtained by means of the radial component for both the models, recalling that $\bar{u}^* \ll \bar{u}^*_{BR} = \bar{v}^*_{BR}$. The RNG k–ϵ model overestimates the radial component modulus of the characteristic velocity for the sections closer to the inlet, while it underestimates the same quantity proceeding along the mini/micro channel. Despite the fact that density fluctuations strongly effect the radial velocity component, as it is evident recalling that $\bar{v} \approx -\bar{v}^*$, the final result on the average heat transfer coefficients is quite moderate. These results confirm that the boundary layer theory can be suitably applied in the present application.

5. Conclusions

A new approach to take into account the effects on turbulence of variable physical properties due to closeness to the critical point has been proposed, by generalizing the decomposition originally considered by the model of Bellmore and Reid. This approach allows us to freely choose the turbulence model for usual terms coming from time averaging of velocity fluctuations and to describe coherently the additional terms due to density fluctuations.

Numerical calculations based on the proposed approach and on the original model have been performed for carbon dioxide flowing within mini/micro channels under cooling conditions. In comparison with existing calculations, some improvements have been considered: an updated database for thermophysical properties near the critical point; some differential equations to investigate the effects of variable thermophysical properties on turbulence; different turbulence closure models for usual terms and for additional terms due to density fluctuations. These refinements do not substantially improve the existing results. This means that for the considered application the effects due to density fluctuations are smaller than it could have been initially supposed on the basis of some interpretations [13]. The comparison with phenomenological correlations confirms that a heat transfer impairment for mini/micro channels exists but it is smaller than the impairment which has been measured by some experiments. The results are not completely exhaustive because of the discrepancies among different correlations due to the coupling between heat transfer and fluid flow. For this reason, some recent attempts [41] to adopt a neural network regression technique in order to interpolate the experimental results concerning the convective heat transfer near the critical point appear greatly promising.

Acknowledgements

The author would like to acknowledge Prof. Michele Calì for creating the conditions for the development of the present work. This work was sponsored by Microtecnica s.r.l., a Hamilton Sundstrand company.

References

[1] G. Lorentzen, J. Pettersen, A new efficient and environmentally benign system for car air-conditioning, Int. J. Refrigeration 16 (1) (1993) 4–12.
[2] J. Pettersen, A. Hafner, G. Skaugen, Development of compact heat exchangers for CO_2 air-conditioning systems, Int. J. Refrigeration 21 (3) (1998) 180–193.
[3] O.K. Rice, Critical phenomena, in: F.D. Rossini (Ed.), Thermodynamics and Physics of Matter, Princeton University Press, Princeton, NJ, 1955, pp. 419–499 (E).
[4] J. Millat, J.H. Dymond, C.A. Nieto de Castro, Transport Properties of Fluids, Cambridge University Press, Cambridge, United Kingdom, 1996.
[5] S. Kakaç, The effect of temperature-dependent fluid properties on convective heat transfer, in: S. Kakaç, R.K. Shah, W. Aung (Eds.), Handbook of Single-phase Convective Heat Transfer, Wiley, New York, 1987, pp. 18.1–18.56.
[6] B.S. Petukhov, Heat transfer and friction in turbulent pipe flow with variable physical properties, Adv. Heat Transfer (6) (1970) 503–565.
[7] S.S. Pitla, D.M. Robinson, E.A. Groll, S. Ramadhyani, Heat transfer from supercritical carbon dioxide in tube flow: a critical review, Int. J. Heating Ventilating Air-Conditioning Refrigerating Res. 3 (4) (1998) 281–301.
[8] E.A. Krasnoshchekov, I.V. Kuraeva, V.S. Protopopov, Local heat transfer of carbon dioxide at supercritical pressure under cooling conditions, High Temp. (translated from Teplofizika Vysokikh Tempeartur) 7 (5) (1970) 856–862.
[9] V.L. Baskov, I.V. Kuraeva, V.S. Protopopov, Heat transfer with the turbulent flow of a liquid at supercritical pressure in tubes under cooling conditions, High Temp. (translated from Teplofizika Vysokikh Tempeartur) 1 (15) (1977) 96–102.
[10] N.E. Petrov, V.N. Popov, Heat transfer and resistance of carbon dioxide being cooled in the supercritical region, Therm. Eng. (translated from Teploenergetika) 32 (3) (1985) 16–19.
[11] J. Pettersen, R. Rieberer, A. Leister, Heat transfer and pressure drop characteristics of supercritical carbon dioxide in microchannel tubes under cooling, International Institute of Refrigeration Commissions B1, B2, E1 and E2, Purdue University Press, 2000, pp. 99–106.
[12] S.V. Pitla, E.A. Groll, S. Ramadhayani, New correlation for the heat transfer coefficient during in-tube cooling of turbulent supercritical carbon dioxide, International Institute of Refrigeration Commissions B1, B2, E1 and E2, Purdue University Press, 2000, pp. 259–267.
[13] S.M. Liao, T.S. Zhao, Measurements of heat transfer coefficients from supercritical carbon dioxide flowing in horizontal mini/micro channels, J. Heat Transfer 124 (2002) 413–420.
[14] J.D. Jackson, W.B. Hall, Influences of buoyancy on heat transfer to fluids flowing in vertical tubes under turbulent conditions, Turbulent Forced Convection in Channels and Bundles, Hemisphere, New York, 1979.

[15] S.H. Yoon, J.H. Kim, Y.W. Hwang, M.S. Kim, K. Min, Y. Kim, Heat transfer and pressure drop characteristics during the in-tube cooling process of carbon dioxide in the supercritical region, Int. J. Refrigeration 26 (2003) 857–864.
[16] V.N. Popov, N.E. Petrov, Calculation of heat transfer and flow resistance in the turbulent pipe flow of cooled carbon dioxide in the supercritical region, High Temp. (translated from Teplofizika Vysokikh Tempeartur) 23 (2) (1985) 309–316.
[17] V.N. Popov, E.P. Valueva, Heat transfer and turbulent flow of water at supercritical parameters if state in a vertical tube with significant effect of free convection, Therm. Eng. (translated from Teploenergetika) 33 (1986) 22–29.
[18] W.B. Hall, Heat transfer near the critical point, Adv. Heat Transfer 7 (1981) 1–83.
[19] S.B. Pope, Turbulent Flows, Cambridge University Press, Cambridge, 2000.
[20] H. Schlichting, Boundary Layer Theory, fourth ed., McGraw-Hill, New York, 1960.
[21] R.G. Deissler, C.S. Eian, Analytical and experimental investigation of fully developed turbulent flow of air in a smooth tube with heat transfer with variable fluid properties, NACA TN 2629, 1952.
[22] V.S. Sastry, N.M. Schnurr, An analytical investigation of forced convection heat transfer to fluids near the thermodynamic critical point, J. Heat Transfer 97 (2) (1975) 226–230.
[23] K. Goldmann, Heat transfer to supercritical water and other fluids with temperature dependent properties, Chem. Eng. Progr. Symp. 50 (11) (1954) 105–113.
[24] C.P. Bellmore, R.L. Reid, Numerical prediction of wall temperatures for near-critical *para*-hydrogen in turbulent upflow inside vertical tubes, J. Heat Transfer 105 (1983) 536–541.
[26] B.E. Launder, D.B. Spalding, Lectures in Mathematical Models of Turbulence, Academic Press, London, 1972.
[27] H.K. Versteeg, W. Malalasekera, An Introduction to Computational Fluid Dynamics: the Finite Volume Method, Addison-Wesley, London, 1996.
[28] V. Yakhot, S.A. Orszag, Renormalization group analysis of turbulence: I. Basic theory, J. Sci. Comput. 1 (1) (1986) 1–51.
[34] E.W. Lemmon, M.O. McLinden, D.G. Friend, Thermophysical properties of fluid systems, in: P.J. Linstrom, W.G. Mallard (Eds.), NIST Chemistry WebBook, National Institute of Standards and Technology, 2003.
[35] J.H. Ferziger, M. Peric, Computational Methods for Fluid Dynamics, Springer-Verlag, Berlin, 1996.
[36] S.V. Patankar, Numerical Heat Transfer and Fluid Flow, Hemisphere, New York, 1980.
[37] S.H. Lee, J.R. Howell, Turbulent developing convective heat transfer in a tube for fluids near the critical point, Int. J. Heat Mass Transfer 41 (10) (1998) 1205–1218.
[38] R.D. Wood, J.M. Smith, Heat transfer in the critical region—temperature and velocity profiles in turbulent flow, A.I.Ch.E. Journal 10 (2) (1964) 180–186.
[39] G.E.P. Box, W.G. Hunter, J.S. Hunter, Statistics for Experimenters, John Wiley & Sons, New York, 1978.
[40] P. Asinari, L. Cecchinato, E. Fornasieri, Effects of thermal conduction in microchannel gas coolers for carbon dioxide, Int. J. Refrigeration 27 (2004) 577–586.
[41] G. Scalabrin, L. Piazza, M. Condosta, Convective cooling of supercritical carbon dioxide inside tubes: heat transfer analysis through neural network, Int. J. Heat Mass Transfer 46 (2003) 4413–4425.